Clay Minerals (2023), **58**, 345–352
doi:10.1180/clm.2023.31

CAMBRIDGE UNIVERSITY PRESS

Short Paper

Preparation of phase-change microcapsules with illite as a filler and their applications in foaming materials

Ming Li, Shuhua Zhang, Weijun Liu, Binyan Liu and Yu Wang

College of Chemistry and Chemical Engineering, Shanghai University of Engineering Science, Shanghai, China

Abstract

To solve the problem of the leakage of phase-change materials and expand the application of clay minerals in the field of phase-change materials, illite and paraffin wax were used for the first time as a new binary hybrid core material with silica as the wall material. Phase-change microcapsules were prepared using the sol–gel method and successfully applied in silicone rubber foams. Differential scanning calorimetry showed that the microcapsules had a melting temperature of 62.99°C and a latent heat capacity of 98.24 J g^{-1}, indicating their good heat-storage capacity. Furthermore, the effectiveness of using illite as a filler for preventing paraffin leakage was demonstrated through 200 thermal cycling tests, which demonstrated a leakage rate of only 2.6% compared to 3.2% exhibited by microcapsules without illite.

Keywords: Clay mineral, illite, phase-change microcapsule

(Received 15 July 2023; revised 23 September 2023; accepted 31 October 2023; Accepted Manuscript online: 6 November 2023; Associate Editor: Chun Hui Zhou)

The progress in clay science is of considerable importance for solving environmental pollution and energy problems (Kaufhold *et al.*, 2019). Therefore, at present, expanding the types and application areas of clay minerals should be considered an important research direction (Zheng *et al.*, 2010). Clay minerals are produced *via* the chemical weathering of silicate minerals on the Earth's surface, and the development and study of clay-based mineral resources provide a scientific basis for exploring the evolutionary laws of the Earth's crustal surface (Lu & Wang, 2022). Because of their superior adsorption capacities, clays have developed as effective and safe scavengers for pollutant removal (Largo *et al.*, 2020; Qiu *et al.*, 2021; Zhou *et al.*, 2023). However, naturally occurring clay minerals contain high levels of impurities, thereby limiting their potential for application. Synthesis techniques have enabled an in-depth understanding of the specific compositions and properties of clay minerals, resulting in the development of novel applications (Sun *et al.*, 2014).

With the development of nanotechnology, application of smectite as a natural nanomaterial has attracted the interest of a wide range of researchers with the aim of utilizing their nanoscale layer spaces to develop highly novel functional composites (Tanboonchuy *et al.*, 2012; Maitlo *et al.*, 2019; Jiang *et al.*, 2021). Currently, composites based on clay minerals have been successfully applied in high-end fields such as adsorbents and cosmetics (Tanboonchuy *et al.*, 2012; Ezati *et al.*, 2021).

Compared to other smectites, such as montmorillonite and kaolinite, the application field of illite is developing, and demand for high-end illite-finished products is increasing. Ilmenite has high potassium and aluminium contents, a small particle size, a large specific surface area and good corrosion resistance, adsorption, heat resistance and plasticity. Therefore, ilmenite has been used in several fields, and its development and utilization prospects are broad. To solve the phase-change microcapsule core leakage problem, researchers have used hybrids of two or more materials as phase-change cores, which improved the thermal-storage efficiency of the microcapsules whilst reducing the liquid-phase leakage of the cores. Zhang *et al.* (2019) prepared a high-temperature-resistant microcapsule with a high encapsulation rate by using a binary mixture of lithium carbonate and sodium carbonate as the core material and the inorganic material silica (SiO_2) as the wall material.

Herein, for the first time, the preparation and synthesis of phase-change microcapsules with SiO_2 as the inorganic shell layers and paraffin (Pa) wax and illite as the phase-change core materials were proposed. This provides a novel opportunity for exploring the application of a smectite in the field of microcapsules and expands the development of clay minerals in the field of phase-change materials. Furthermore, these microcapsules can be successfully applied in silicone rubber foam (SRF), which is a material with good elasticity and toughness and is widely used for providing support to building structures. For example, Guo *et al.* (2019) prepared a morphologically stable composite foam SRF/Pa@SiO_2, in which SiO_2 acts as a shell material to provide barrier protection for the phase-change core material Pa and as an inorganic filler to enhance the mechanical strength of SRF. Lou *et al.* (2020) introduced Pa@lead tungstate microcapsules into foam substrates with SRF as the carrier, and these researchers were able to prepare composite phase-change foams with relatively stable shapes.

Materials and methods

Raw materials and chemical reagents

Pa (solid), cetyltrimethylammonium bromide (CTAB; powder), hydrochloric acid (liquid) and tetraethyl silicate (TEOS; liquid)

Corresponding author: Shuhua Zhang; Email: zsh_7474@126.com
Cite this article: Li M, Zhang S, Liu W, Liu B, Wang Y (2023). Preparation of phase-change microcapsules with illite as a filler and their applications in foaming materials. *Clay Minerals* **58**, 345–352. https://doi.org/10.1180/clm.2023.31

were purchased from Sinopharm Chemical Reagents Ltd (Shanghai, China). A 2000-grade illite powder (2000 mesh powder) was sourced from Antu County, Yanbian, Jilin Province, China. Liquid silicone rubber (107-LSR), E620-A (liquid), E620-B (liquid), hydrogen-containing silicone oil (liquid) and methyl silicone oil (liquid) were obtained from China Jinan Feng Chemical Co., Ltd (Jinan, China).

Modification

The crystal structure of illite primarily comprises a layer of aluminium–oxygen octahedra sandwiched between two layers of silicon–oxygen tetrahedra, with hydroxyl groups present on the surface and edges of this lamellar structure, and it has a chemical formula $K_{1-1.5}Al[Si_{6.5-7}Al_{1-1.5}O_{20}](OH)_4$. Illite was modified as follows: purified illite, CTAB and distilled water were mixed well and stirred at 60°C for 30 min in a magnetic stirrer, washed three times and dried. The modification mechanism occurred mainly through an ion-exchange reaction between the interlayer cations of illite and cationic surfactants using the alkyl chains in the surfactant structure to reduce the hydrophilicity and increase the lipophilicity of illite. This ensures that a tight connection can be made with the Pa (Wang *et al.*, 2021).

Preparation of phase-change microcapsules

Illite–CTAB (0.2 g) and distilled water (100 mL) were thoroughly mixed and then ultrasonicated, heated and stirred. Subsequently, this mixed solution was added to a Pa (9.8 g) emulsion and allowed to emulsify for 2 h. An encapsulated precursor solution was obtained *via* combining TEOS (10 g) and distilled water (20 g) in a beaker and adjusting the pH of the mixture to between 2 and 3 using hydrochloric acid. Then, the solution was incrementally added to the Pa emulsion and stirred for 4 h at 70°C. Finally, the white powder was collected on filter paper, washed three times with hot anhydrous ethanol and dried at 25°C. The resulting solid powder is the microencapsulated Pa@SiO_2@illite–CTAB.

Preparation of the composite phase-change foam materials

107-LSR, hydrogenated silicone oil, methyl silicone oil and E620-B were mixed to obtain component A and 30 wt.% E620-A catalyst and Pa@SiO_2@illite–CTAB were mixed to obtain component B. The mixtures were stirred and placed in an oven to obtain SRF. The preparation of SRF/Pa@SiO_2@illite–CTAB is depicted in Fig. 1.

Characterization and performance analysis

Characterization

The morphology of the prepared microcapsules was observed using optical microscopy (OM; D106B, Dongwan, China). The microstructures of the microcapsules and composite foam samples were observed using scanning electron microscopy (SEM; SU8010, Shanghai, China). Elemental analysis of the samples was obtained using Fourier-transform infrared (FTIR) spectrometry (370 IS10; Thermo Fisher Scientific, Shanghai, China) in attenuated total reflectance mode in the 4000–500 cm^{-1} range. X-ray photoelectron spectroscopy (XPS; K-Alpha, Thermo Fisher

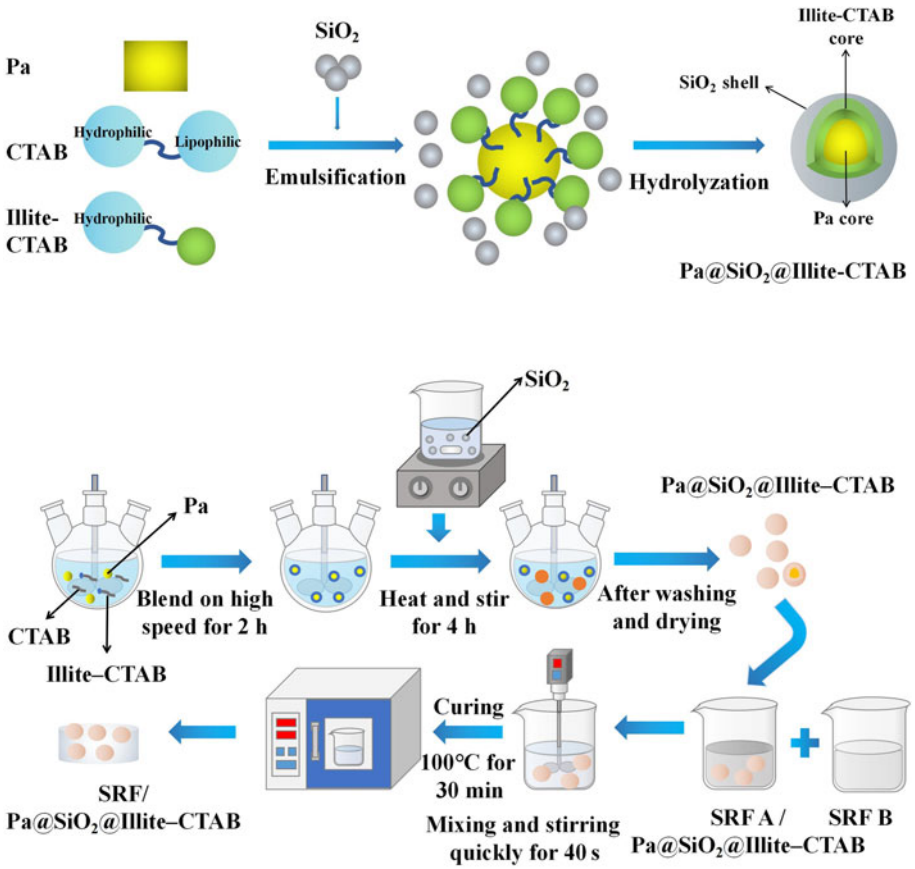

Figure 1. Preparation of Pa@SiO_2@illite–CTAB and SRF/Pa@SiO_2@illite–CTAB.

https://doi.org/10.1180/clm.2023.31 Published online by Cambridge University Press

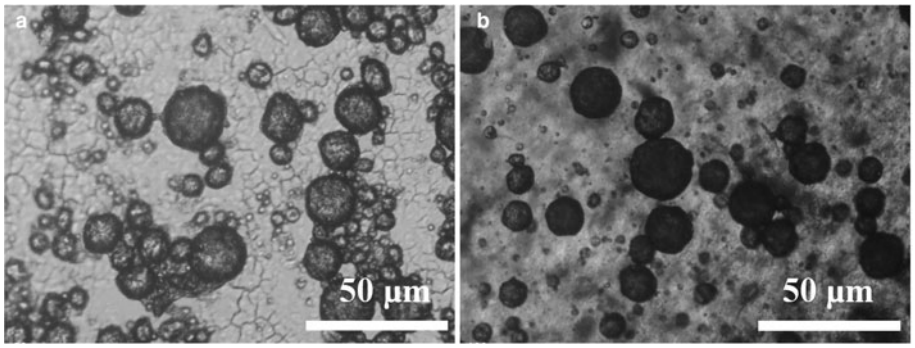

Figure 2. OM images of (a) Pa@SiO_2 and (b) Pa@SiO_2@illite–CTAB.

Scientific, Shanghai, China) was used to analyse the elements on the microcapsule surface. The crystal structure of the microcapsules was characterized using X-ray diffraction (XRD; Rigaku Ultima IV, Thermo Fisher Scientific, Shanghai, China) in the range of 5–90° with a scanning speed of 10° min^{-1}. The thermal properties were analysed using differential scanning calorimetry (DSC; DSC 25, TA Instruments, Inc., Shanghai, China) at a heating rate of 10°C min^{-1} from 30°C to 70°C under a nitrogen atmosphere with a holding time of 5 min. The thermal stability was analysed using thermogravimetric analysis (TGA; EXSTRA 6300, Shanghai, China) at a heating rate of 20°C min^{-1} from 25°C to 800°C in a synthetic air atmosphere (50 mL min^{-1}).

Performance analysis

The thermal conductivities of the composite foam samples were measured using the transient plane method with a thermal conductivity tester (DRE-III, Shanghai, China) at room temperature and averaged over several tests per sample. Heat transfer experiments for the composite foam materials were performed in an environmental chamber. Leakage rate experiments for the composite foams were performed in an oven at a temperature (75°C) higher than the melting point of Pa. The initial weight of the samples is represented as m_0, and their subsequent weight is represented as m_n. The equation for calculating the leakage rate (μ) is shown in Equation 1 (Zuo *et al.*, 2020):

$$\mu = \left(\frac{m_0 - m_n}{m_0}\right) \times 100\% \quad (1)$$

where μ is the leakage rate, m_0 is the initial weight of the experimental sample and m_n is the weight of the nth heating at 75°C.

Results and discussion

Optical microscopy

Figure 2 illustrates the microstructures of Pa@SiO_2 and Pa@SiO_2@illite–CTAB observed via OM. The dispersion of the microspheres is mostly uniform, and the particle size ranges from 10 to 50 μm.

FTIR spectroscopy

Figure 3 shows the FTIR spectra for Pa, SiO_2, illite–CTAB, Pa@SiO_2 and Pa@SiO_2@illite–CTAB. The peaks at 2915 and 2841 cm^{-1} correspond to the stretching vibrations of CH_3 and CH_2, respectively (Zhang *et al.*, 2022). Moreover, these peaks appear in the FTIR spectrum of illite–CTAB, suggesting that illite was successfully modified using CTAB. The peaks at 1460 and 1374 cm^{-1} correspond to the deformed vibrational peaks of CH_2 and CH_3, respectively. The absorption bands at 3000–3600 and 1600–1700 cm^{-1} correspond to the stretching and bending vibrations of the –OH functional group in SiO_2, respectively. The bending vibrations of the Si–O functional group are observed at 1040 and 798 cm^{-1}. The peak at 948 cm^{-1} corresponds to the Si–OH group.

Since SiO_2 can only be formed at paraffin interfaces, the FTIR spectroscopy results indicate that SiO_2 shells are formed on the surface of paraffin droplets (Fang *et al.*, 2010). In the FTIR spectra of Pa@SiO_2 and Pa@SiO_2@illite–CTAB, there was no change in the absorption peaks at 2920, 2850, 1460 and 719 cm^{-1} for paraffin. This result demonstrates that there is no chemical interaction between the Pa molecule and SiO_2.

XPS analysis

To further understand the content of illite in the Pa@SiO_2@illite–CTAB microcapsules, the elements of Pa@SiO_2@illite–CTAB were analysed using XPS. The elemental composition of the microcapsules comprises C, O, Si and Al (Fig. 4a). The C binding mode of Pa@SiO_2@illite–CTAB was investigated *via* curve fitting the high-resolution spectrum of C 1s, as shown in Fig. 4b. The 284.4 and 286.0 eV peaks of C 1s, corresponding to C–C or C=O and C–O, were attributed to the Pa in the microcapsules (Atri *et al.*, 2020). The fitted curve of the Si 2p energy band is shown in Fig. 4c. The

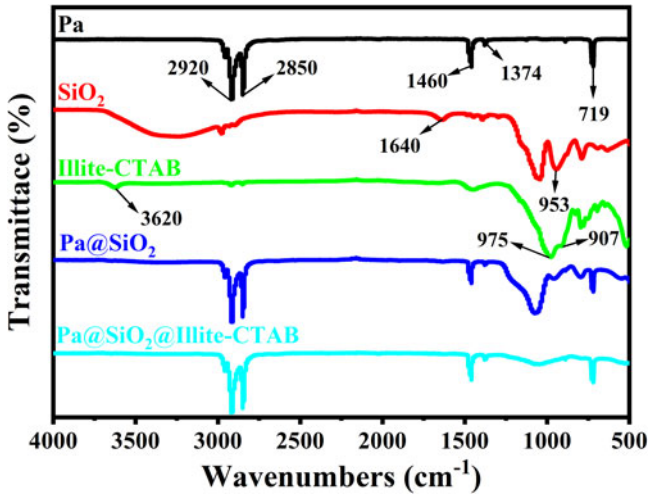

Figure 3. FTIR spectra of Pa, SiO_2, illite–CTAB, Pa@SiO_2 and Pa@SiO_2@illite–CTAB.

https://doi.org/10.1180/clm.2023.31 Published online by Cambridge University Press

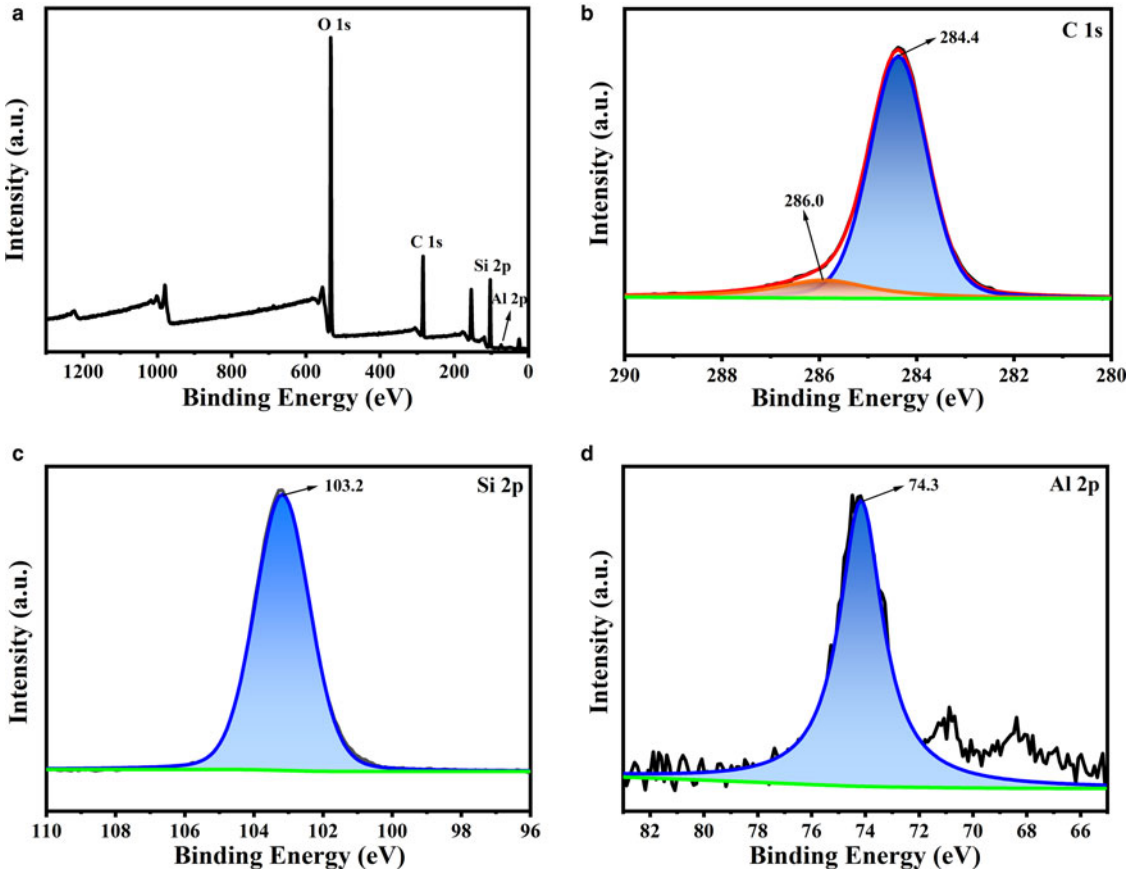

Figure 4. XPS analysis: (a) full-spectrum scan, (b) C 1s, (c) Si 2p and (d) Al 2p.

main peak at 103.2 eV corresponds to the binding energy of O–Si–O, confirming the presence of SiO_2 microspheres in the microcapsules. The curves shown in Fig. 4d suggest that the peaks at 74.3 and 68.5 eV correspond to the Al 2p signal peaks (Hu *et al.*, 2012), which are mainly attributed to the aluminium present in illite. The ratio of Al to Si in illite is 1:5, and that in the microcapsules is 1:8 (Table 1), indicating that SiO_2 microspheres exist on the microcapsule surface, in addition to illite. Combining the FTIR spectroscopy results of the microcapsules reveals that SiO_2 was successfully encapsulated on the microcapsule surface.

XRD analysis

Figure 5 shows the XRD spectra of Pa, SiO_2, illite–CTAB, Pa@SiO_2 and Pa@SiO_2@illite–CTAB. As can be seen from Fig. 5, the regular crystallization of Pa occurs at 21.47° and 23.79°. SiO_2 has a flat peak in the 2θ range of 20–25°, indicating that SiO_2 has an amorphous structure and has the conditions to form microcapsule shells. The characteristic diffraction peaks of the XRD spectrum of illite–CTAB at 2θ = 8.91° and 20.23° correspond to the crystallographic indices (002) and (006), respectively.

Table 1. Elemental contents of C, O, Si and Al in Pa@SiO_2@illite–CTAB.

Element	C 1s	O 1s	Si 2p	Al 2p
Elemental content (%)	25.58	40.75	24.32	2.68

The XRD peaks of Pa in Pa@SiO_2 and Pa@SiO_2@illite–CTAB are based on the SiO_2 flat peaks shown. However, due to the low content of illite in the microcapsules, no characteristic peaks belonging to illite were observed in the XRD spectra of Pa@SiO_2@illite–CTAB. In addition, there are no other diffraction peaks in the XRD spectrum of Pa@SiO_2@illite–CTAB, so the microencapsulation of Pa does not change its crystalline structure, which ensures that the microcapsule still has a good thermal-storage capacity and can be thermally managed by the solid–liquid phase transition.

SEM analysis

SEM images of Pa@SiO_2/illite, Pa@SiO_2@illite–CTAB, SRF and SRF/Pa@SiO_2@illite–CTAB are shown in Fig. 6. To prove that the illite was successfully modified using CTAB, microencapsulated Pa@SiO_2/illite was prepared using unmodified illite instead of illite–CTAB. As shown in Fig. 6a,b, unmodified illite was heavily agglomerated with Pa@SiO_2 microspheres, and the microsphere surface was smooth without illite attached. Lipophilicity of illite–CTAB increased due to the presence of alkyl chains on the CTAB structure, ensuring that illite forms strong bonds with Pa (Wang *et al.*, 2021). Therefore, the illite unmodified by CTAB was directly added to the preparation of the microcapsules, and illite existed in the system in an independent state, also proving that the modification of Illite by CTAB was successful.

As detailed in Fig. 6c,d, Pa@SiO_2@illite–CTAB exhibited a distinct spherical microstructure, and its surface revealed the laminar

https://doi.org/10.1180/clm.2023.31 Published online by Cambridge University Press

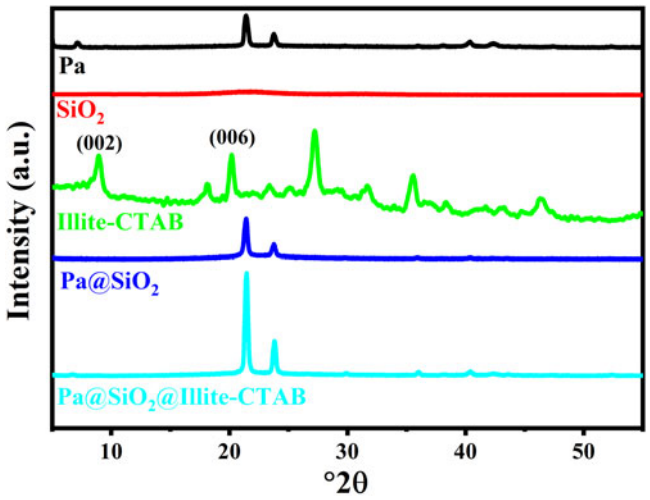

Figure 5. XRD spectra of Pa, SiO_2, illite–CTAB, Pa@SiO_2 and Pa@SiO_2@illite–CTAB.

structure of the illite that was not encapsulated by silica. Combined with FTIR and XRD analyses, it can be observed that in the Pa@SiO_2@illite–CTAB system, SiO_2 generated from the hydrolysis of TEOS is spread on the surface of the paraffin droplets, and strong bonds are generated between the illite–CTAB and the Pa to form a heterogeneous core, with the illite acting as a filler to be distributed in the core. As detailed in Fig. 6e,f, the blank SRF exhibits a uniform circular vesicle structure, and the microcapsules are well dispersed within the pore structures of the composite foam and did not break.

Phase-change temperature and latent heat capacity

The phase-change temperatures were denoted as the melting temperature (T_m) and crystallization temperature (T_c), and the phase-change enthalpies were denoted as the enthalpy of melting (H_m) and the enthalpy of crystallization (H_c). Figure 7 shows the phase-change temperatures and enthalpies for all of the samples. Furthermore, the DSC curves exhibit two heat-absorption peaks and two heat-release peaks, wherein the primary and secondary peaks indicate solid–liquid and solid–solid processes, respectively. Both Pa@SiO_2@illite–CTAB and SRF/Pa@SiO_2@illite–CTAB exhibit excellent phase-change capabilities, with enthalpies of 98.24 and 16.91 J g^{-1}, respectively. The increase in T_m and slight decrease in T_c for Pa@SiO_2@illite–CTAB compared to Pa and Pa@SiO_2 are primarily attributed to the presence of large amounts of illite within the silica shell layer.

Thermal stability analysis

The TGA and differential thermogravimetry (DTG) curves of the Pa, Pa@SiO_2, Pa@SiO_2@illite–CTAB and composite phase-change foams are shown in Fig. 8a,b. Pa exhibits a typical one-step

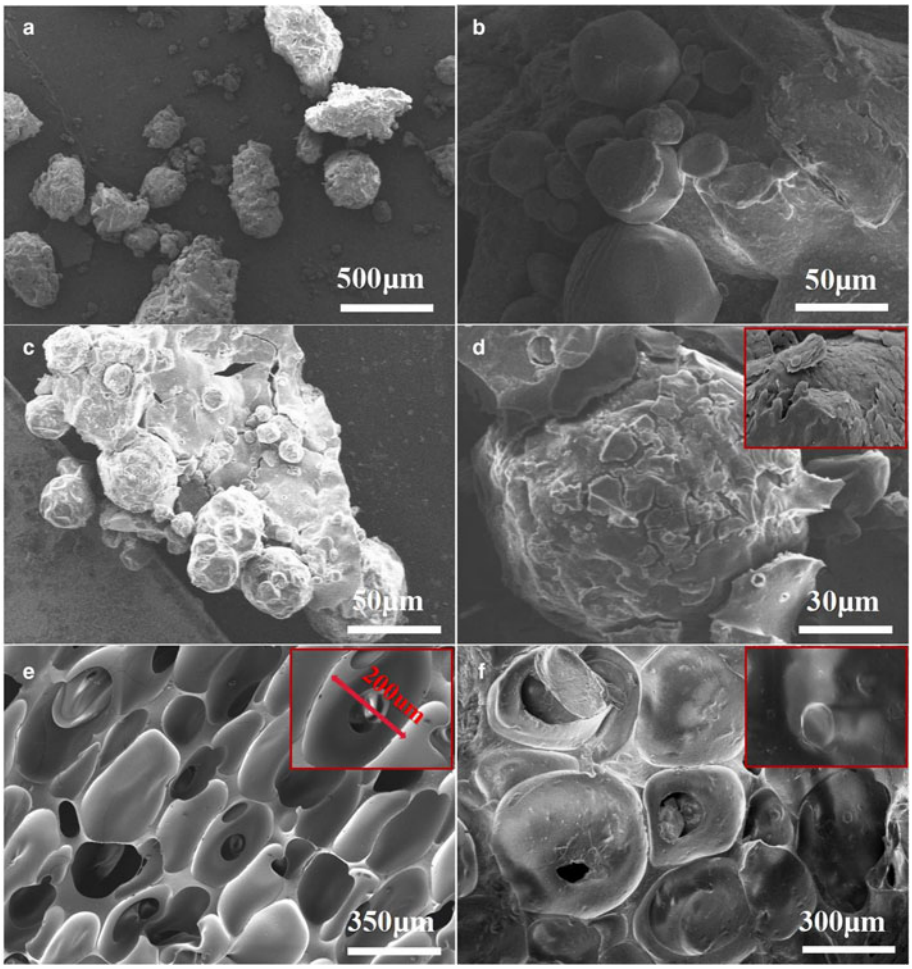

Figure 6. SEM images of (a,b) Pa@SiO_2/illite, (c,d) Pa@SiO_2@illite–CTAB, (e) SRF and (f) SRF/Pa@SiO_2@illite–CTAB.

https://doi.org/10.1180/clm.2023.31 Published online by Cambridge University Press

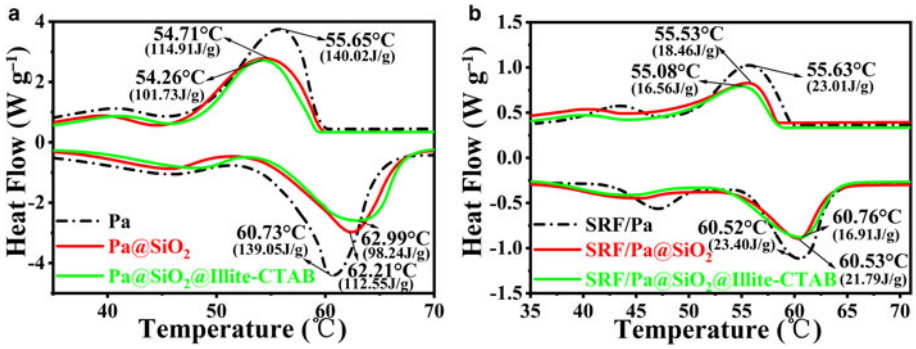

Figure 7. DSC of (a) Pa, Pa@SiO_2 and Pa@SiO_2@illite–CTAB and (b) SRF/Pa, SRF/Pa@SiO_2 and SRF/Pa@SiO_2@illite-CTAB.

thermal decomposition process, with thermal decomposition starting at 102°C and finishing at ~257°C. The thermal decomposition temperatures of Pa@SiO_2 and Pa@SiO_2@illite–CTAB are 127°C and 135°C, respectively, and their residual masses are 26.02% and 32.46%, respectively, after combustion. This is due to the protective effect of the SiO_2 shell on the core material, which slows down the thermal degradation of Pa. Additionally, illite–CTAB increases the thermal decomposition temperature of the microcapsules. The composite foams exhibit a two-step thermal degradation process: the first step occurs between 100°C and 300°C, corresponding to the thermal decomposition of the Pa molecular chain, and the second step happens between 500°C and 700°C, attributed to the thermal degradation of SRF.

Leakage rate analysis

In addition, a composite foam, SRF/Pa/illite–CTAB, was prepared using equal proportions of Pa@SiO_2@illite–CTAB and illite–CTAB. Figure 9 shows the digital images of the composite phase-change foam before and after 200 thermal cycles with its leakage rate variation curve. The leakage rate for SRF/Pa is 11.9%, whereas those of SRF/Pa@SiO_2 and SRF/Pa@SiO_2@illite–CTAB are 3.2% and 2.6%, respectively. Pa@SiO_2@illite–CTAB exhibits excellent low leakage rates and recyclability. Thermal cycling experiments for over 200 cycles demonstrate that illite–CTAB as a microcapsule core material could effectively prevent the Pa liquid phase from leaking.

Thermal conductivity

The thermal conductivities of the Pa, SRF and composite phase-change foams are presented in Fig. 10. The thermal conductivity of the composite foam SRF/Pa@SiO_2@illite–CTAB is reduced to 0.1138 W (m·K)$^{-1}$, and SRF/Pa@SiO_2 exhibits a higher value of 0.1568 W (m·K)$^{-1}$. Moreover, the presence of a large amount of illite as a filler in the microcapsule core causes decrease in the rates of heating and cooling, reducing the thermal conductivity of the composite foam. Therefore, this composite foam is suitable for application in the field of insulation.

Analysis of heat transfer characteristics

The heat transfer tests on the foam samples, which were conducted in an environmental chamber, employed the following procedure: the foam samples were placed on a 100°C temperature-controlled rubber heating plate, a K-type thermocouple was attached to the surface of the foam and the temperature was recorded using an Agilent data acquisition system.

Temperature–time graphs of the collected data are shown in Fig. 11. The temperature–time curves of all of the composite foams plateau between 350 and 1340 s. These plateaus arise due to the latent heat absorption of Pa at its phase-change temperature, resulting in the substantial delay of a temperature increase. In contrast to the SRF/Pa, SRF/Pa@SiO_2 and SRF/Pa/illite–CTAB profiles, the plateau of the composite foam material with SRF/Pa@SiO_2@illite–CTAB persists for longer. This is primarily due to the replacement of a portion of the core Pa by illite–CTAB, resulting in high hysteresis in the Pa heat uptake.

The results of the heat transfer tests confirm that illite–CTAB as a filler for the microcapsule core does not change the microcapsule phase-change properties whilst offering considerably enhanced temperature regulation stability.

Hardness analysis

The hardness of the composite foam materials SRF, SRF/Pa, SRF/Pa@SiO_2, SRF/Pa@SiO_2@illite–CTAB and SRF/Pa/illite–CTAB were tested and analysed, as shown in Fig. 12. The hardness of

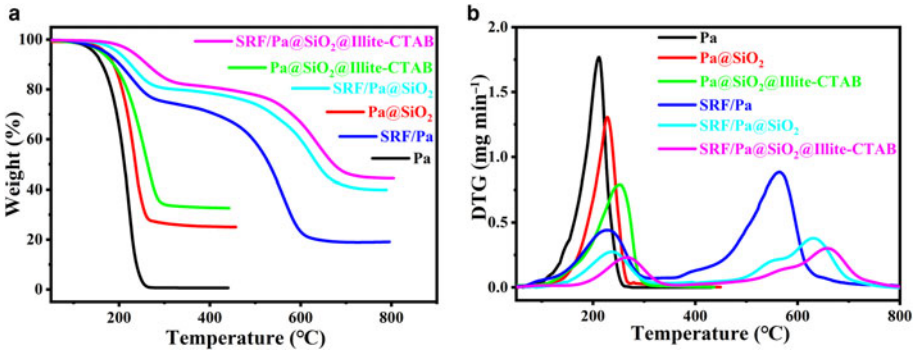

Figure 8. (a) TGA and (b) DTG curves for Pa, Pa@SiO_2, Pa@SiO_2@illite–CTAB, SRF/Pa, SRF/Pa@SiO_2 and SRF/Pa@SiO_2@illite–CTAB.

https://doi.org/10.1180/clm.2023.31 Published online by Cambridge University Press

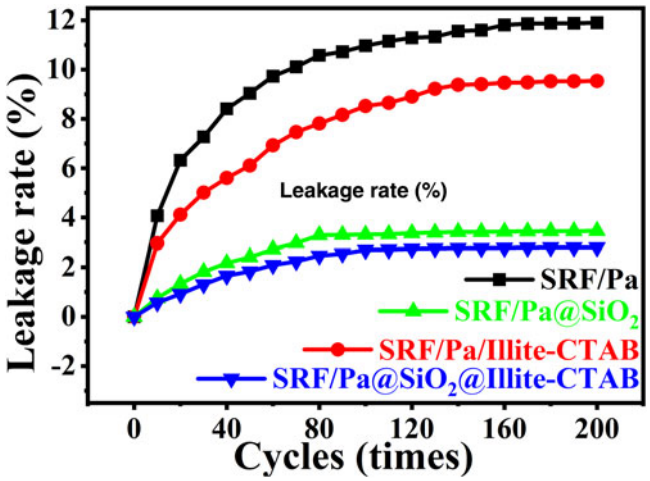

Figure 9. Thermal cycle test over 200 cycles: leakage rate curves.

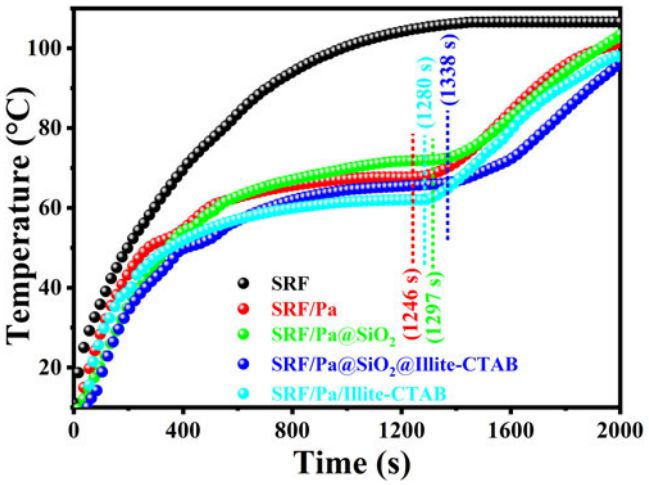

Figure 11. Temperature–time curves of SRF, SRF/Pa, SRF/Pa@SiO_2, SRF/Pa@SiO_2@illite-CTAB and SRF/Pa/illite-CTAB.

the blank SRF foamed material is 2.73 HC, and the hardness of the composite SRF/Pa after the addition of Pa is 2.89 HC. Combined with the results from the SEM analysis of the SRF/Pa composite foam material, the majority of the SRF vesicles were determined to be filled with Pa, increasing the hardness of SRF/Pa. However, the hardness of the SRF/Pa@SiO_2@illite–CTAB composite material is greater.

The presence of illite in the core portion of the microcapsule increases the hardness of the microcapsule and SRF/Pa@SiO_2@illite–CTAB foam.

Conclusion

In this study, a new thermal storage microcapsule, Pa@SiO_2@illite–CTAB, was successfully prepared using illite as the core filler. The complete structure of the Pa@SiO_2@illite–CTAB system, with SiO_2 as the encapsulated shell and Pa and illite–CTAB as the hybridized core materials, was clarified using FTIR spectroscopy, XRD and SEM characterizations. Characterization experiments such as 200 rounds of thermal cycling showed that illite was encapsulated as a filler for the core Pa in a silica shell, and the liquid-phase leakage of Pa was significantly reduced. The microencapsulated Pa@SiO_2@illite–CTAB could maintain its intact morphology, good phase-transition characteristics and excellent mechanical properties after being applied to SRF.

In summary, the modified illite could be used as a support material for microcapsule cores for preventing the thermal decomposition and leakage of phase-change cores at room temperature, to improve the thermal stability and strength of microcapsule systems and to achieve effective practical value in the field of phase-change materials. Most of the current research on clay minerals by researchers has been limited to observing the

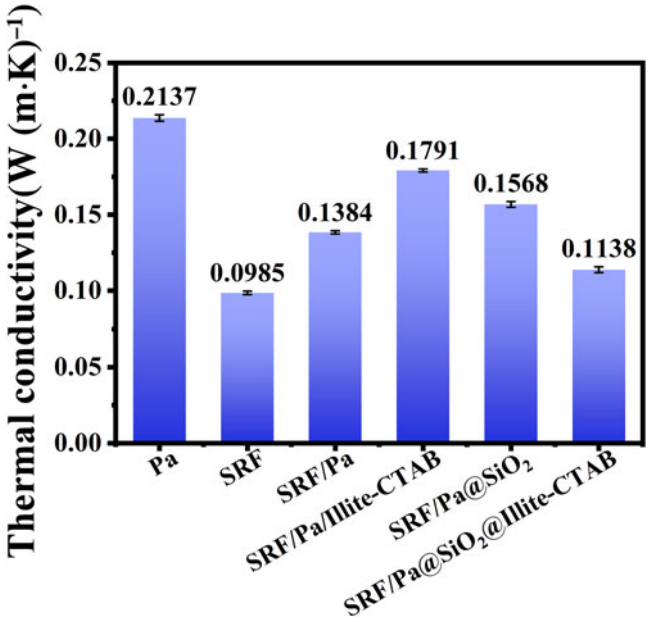

Figure 10. Thermal conductivities of Pa, SRF, and composite phase-change foam materials.

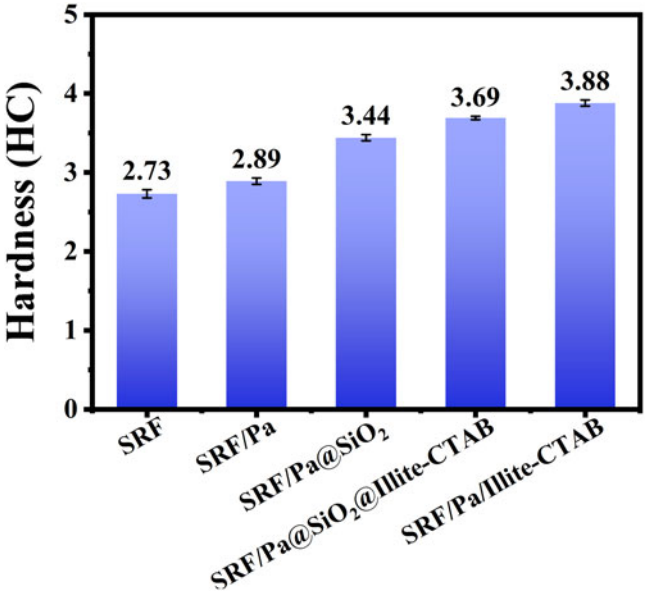

Figure 12. Hardness of SRF, SRF/Pa, SRF/Pa@SiO_2, SRF/Pa@SiO_2@illite–CTAB and SRF/Pa/illite–CTAB.

https://doi.org/10.1180/clm.2023.31 Published online by Cambridge University Press

microstructure of clay pores. Analysing the utilization of the natural adsorption properties of clays in combination with other materials will extend their application value and is a direction worth exploring.

Financial support. This work was supported by the Shanghai University of Engineering Science, Program of Graduate Research Innovation Project (No. 023E4600019grfz004).

Conflicts of interest. The authors declare that they have no known competing financial interests or personal relationships that could have appeared to influence the work reported in this paper.

References

Atri S., Uma S., & Nagarajan R. (2020) Magnetic and photocatalytic properties of nano-sized sulfur-doped trirutile oxide, $CuSb_2O_6$. *Materials Science in Semiconductor Processing*, **119**, 105226.

Ezati P., Bang Y.-J. & Rhim J.-W. (2021) Preparation of a shikonin-based pH-sensitive color indicator for monitoring the freshness of fish and pork. *Food Chemistry*, **337**, 127995.

Fang G., Chen Z., & Li H. (2010) Synthesis and properties of microencapsulated paraffin composites with SiO_2 shell as thermal energy storage materials. *Chemical Engineering Journal*, **163**, 154–159.

Guo Y., Yang W., Jiang Z., He F., Zhang K., He R. *et al.* (2019) Silicone rubber/paraffin@silicon dioxide form-stable phase change materials with thermal energy storage and enhanced mechanical property. *Solar Energy Materials and Solar Cells*, **196**, 16–24.

Hu N., He L.J. & Wang L.H. (2012) Study on surface chemical composition and structure of PVP/Al composite powder using XPS analysis. *Advanced Materials Research*, 476–478, 1101–1104.

Jiang W., Han Y., Jiang Y., Xu F., Ouyang D. & Sun J. (2021) Preparation and electrochemical properties of sepiolite supported Co_3O_4 nanoparticles. *Applied Clay Science*, **203**, 106020.

Kaufhold S., Chryssikos G., Kacandes G., Gionis V., Ufer K. & Dohrmann R. (2019) Geochemical and mineralogical characterization of smectites from the Ventzia basin, western Macedonia, Greece. *Clay Minerals*, **54**, 95–107.

Largo F., Haounati R., Akhouairi S., Ouachtak H., El Haouti R. & El Guerdaoui A. (2020) Adsorptive removal of both cationic and anionic dyes by using sepiolite clay mineral as adsorbent: experimental and molecular dynamic simulation studies. *Journal of Molecular Liquids*, **318**, 114247.

Lou L., He Z., Li Y., Li Y., Zhou Y., Lin C. *et al.* (2020) Multifunctional silicone rubber/paraffin@$PbWO_4$ phase-change composites for thermoregulation and gamma radiation shielding. *International Journal of Energy Research*, **44**, 7674–7686.

Lu Y. & Wang A. (2022) From structure evolution of palygorskite to functional material: a review. *Microporous and Mesoporous Materials*, **333**, 111765.

Maitlo H.A., Kim K.H., Kumar V., Kim S. & Park J.W. (2019) Nanomaterials-based treatment options for chromium in aqueous environments. *Environment International*, **130**, 104748.

Qiu P., Guo L., Qi Y., Cheng M. & Jing Z. (2021) Hydrothermal solidification of sepiolite into a cemented sepiolite aggregate for humidity regulation and formaldehyde removal. *Clay Minerals*, **55**, 320–328.

Sun T., Xiao J.J., Liu Q., Zhao F. & Xiao H.M. (2014) Comparative study on structure, energetic and mechanical properties of a ϵ-CL-20/HMX cocrystal and its composite with molecular dynamics simulation. *Journal of Materials Chemistry A*, **2**, 13898–13904.

Tanboonchuy V., Grisdanurak N. & Liao C.H. (2012) Background species effect on aqueous arsenic removal by nano zero-valent iron using fractional factorial design. *Journal of Hazardous Materials*, **205**, 40–46.

Wang Z., Wang S., Yu X., Zhang H. & Yan S. (2021). Study on the use of CTAB-treated illite as an alternative filler for natural rubber. *ACS Omega*, **6**, 19017–19025.

Zhang H., Shin D. & Santhanagopalan S. (2019). Microencapsulated binary carbonate salt mixture in silica shell with enhanced effective heat capacity for high temperature latent heat storage. *Renewable Energy*, **134**, 1156–1162.

Zhang D., Cai T., Li Y., Li Y., He F., Chen Z. *et al.* (2022) Paraffin@silica microencapsulated phase change materials with improved anti-leakage properties. *ChemistrySelect*, **7**, e202202930.

Zheng S.-Q., Han Y., Huang X.-H., Dai Y.-L., Qian D., Zhang J.-C. & Ren S. (2010) Acid and aluminium modification of sepiolite and its application in FCC catalysis. *Clay Minerals*, **45**, 15–22.

Zhou J., Wang Z., Alcântara A. & Ding Y. (2023) Study of the adsorption mechanisms of NH3, H_2S and SO_2 on sepiolite using molecular dynamics simulations. *Clay Minerals*, **58**, 1–6.

Zuo X., Li J., Zhao X., Yang H. & Chen D. (2020) Emerging paraffin/carbon-coated nanoscroll composite phase change material for thermal energy storage. *Renewable Energy*, **152**, 579–589.

https://doi.org/10.1180/clm.2023.31 Published online by Cambridge University Press